

The Role of Alpha-Methylbenzyl Ammonium Iodide to Reduce Defect Densities in Perovskite Devices

Bekele Hailegnaw, Felix Mayr, Christoph Putz, Lukas Lehner, Katarina Gugujonovic, Stepan Demchyshyn, Martin Kaltenbrunner, and Markus C. Scharber*

Hybrid organic–inorganic perovskite photovoltaic has achieved unmatched power conversion efficiency (PCE) improvement in the last decade. Nevertheless, nonradiative recombination of charge carriers due to bulk and interface defects reduces the open-circuit voltage (V_{OC}) and PCE of perovskite solar cells. Incorporating additives, process optimization, and interface engineering are among the effective approaches employed to reduce such issues. Herein, quasi-2D p–i–n perovskite solar cells incorporating alpha-methylbenzyl ammonium iodide (MBAI) cation with outstanding photovoltaic performance and stability are developed. MBAI incorporation results in films with excellent optical and electrical properties, leading to higher V_{OC} of ≈ 1.15 V, fill factor of above 77%, and stability of the device. A high open-circuit voltage and fill factor and corrected power conversion efficiencies in the range of 15% are obtained for the prepared devices. The encapsulated solar cells show excellent operational stability under white light illumination in ambient air for >500 h. Due to the simple and robust preparation process, the investigated inverted perovskite solar cell can easily be combined with other solution-processed thin film solar cells to form multijunction devices and can easily be integrated into different lightweight and flexible products.


1. Introduction

Perovskite solar cells (PSCs) are the most promising next-generation photovoltaic devices, having outstanding optoelectronic properties and the advantage to fabricate large-area devices under low-temperature processes based on cheaper precursor materials. Not only the scientific community but also several

companies are currently exploring the potential of this technology. First perovskite solar cells with a power conversion efficiency (PCE) of about 3.8% were reported by Miyasaka et al.^[1] Since then, unprecedented improvements in solar cell efficiency have been accomplished through the optimization of the composition and growth of the semiconductor layer, the careful selection of charge transport materials, and the optimization of interfaces in the device.^[2] The current record power conversion efficiencies of perovskite solar cells are on par with the best crystalline silicon solar cell and exceed 25%.^[3] The highest efficiencies are often obtained for solar cells utilizing a mesoporous TiO_2 —acting as an electron-selective transport layer—deposited between the transparent front contact and the absorber layer. This results in a device with an n–i–p configuration. In contrast, so-called inverted PSCs are based on a p–i–n configuration with a hole transport layer (HTL) deposited on the transparent contact, followed by the perovskite absorber, an electron transport layer (ETL), and a metal electrode contact. The p–i–n design offers several advantages. Highly conductive and transparent hole transport materials are available which can also be used as semitransparent contacts when supported with a metal mesh electrode. In this configuration, no transparent conductive oxide (TCO) layer is required on the front side of the solar cell substrate. The preparation of inverted PSCs requires only moderate process temperatures, which make them suitable for deposition on standard plastic substrates. Therefore, inverted PSCs can easily be combined with other solar cells to form multijunction devices and can also be integrated into lightweight and flexible products. Poly(3,4-ethylenedioxythiophene):poly(styrene sulfonate) (PEDOT:PSS) has frequently been used as conductive and transparent hole transport material in perovskite solar cells. It can be processed from solution, has excellent film-forming properties, high transparency in visible light range, high mechanical flexibility, high electrical conductivity, and good air stability. However, first-generation p–i–n perovskite solar cells suffered from severe open circuit voltage (V_{OC}) losses.^[4,5] Interlayer materials like PEDOT:PSS and PCBM lead to a strong quenching of the absorber luminescence induced by rapid surface recombination. Different posttreatment procedures, the addition of dopants, or the application of bilayer

B. Hailegnaw, C. Putz, L. Lehner, S. Demchyshyn, M. Kaltenbrunner
Division of Soft Matter Physics Institute of Experimental Physics
Johannes Kepler University
Altenberger Str. 69, 4040 Linz, Austria

F. Mayr, K. Gugujonovic, M. C. Scharber
Linz Institute for Organic Solar Cells (LIOS) and Institute for Physical Chemistry
Johannes Kepler University
Altenberger Str. 69, 4040 Linz, Austria
E-mail: markus_clark.scharber@jku.at

 The ORCID identification number(s) for the author(s) of this article can be found under <https://doi.org/10.1002/solr.202300316>.

© 2023 The Authors. Solar RRL published by Wiley-VCH GmbH. This is an open access article under the terms of the Creative Commons Attribution-NonCommercial License, which permits use, distribution and reproduction in any medium, provided the original work is properly cited and is not used for commercial purposes.

DOI: 10.1002/solr.202300316

structure have been proposed to overcome the observed V_{OC} losses.^[6–10]

With the development of mixed perovskite absorbers,^[11] the application of surface passivation materials,^[12] and the discovery of 2D/3D perovskite structures^[13,14] the open circuit voltage losses could be significantly reduced, and with this, the PCE of p–i–n devices could be improved.^[15,16] Despite the high PCE, there are still loss processes active in these devices. For further improvements, a detailed understanding of defect states and recombination centers is essential. The diode ideality factor is an important parameter, which characterizes the losses in photovoltaic devices.^[9] It can be determined in different ways requiring no advanced characterization tools. The diode ideality factor is originally defined by the current–voltage (j – V) characteristics of a diode according to $j = j_0(\exp(qV/nkT) - 1)$, with current density j , reverse saturation current density j_0 , unit charge q , the applied voltage V , Boltzmann constant k , temperature T , and diode ideality factor n . The diode ideality factor depends on the dominating recombination mechanism. The classical model by Shockley^[17] considers the injection of minority carriers through the space charge region, which then recombines outside the space charge region within the distance of the diffusion length. Thereby, it is not important whether the recombination takes place radiatively or nonradiatively. The diode ideality factor, in this case, is 1. The other classic example is the Shockley–Read–Hall (SRH) recombination in the space charge region through a defect at mid-gap, where the diode ideality factor becomes 2.^[18] Real solar cells often exhibit ideality factors between 1 and 2 suggesting that various recombination processes need to be considered to be active in the device. A theoretical and experimental study on perovskite solar cells, investigating the effects of bulk and interface recombination on the ideality factor suggest that interfacial recombination leads to a lower n compared to SRH recombination in the bulk.^[19]

In addition, the investigations are used to rationalize that n values between 1 and 2 found in perovskite solar cells can originate exclusively from a single recombination process.^[19,20] The photoluminescence Φ_{PL} of a solar cell depends on the quasi-Fermi-level splitting (μ) in the absorber and is proportional to $(\exp(\mu/(k_B T)))$. In an ideal solar cell, the quasi-Fermi-level splitting and the open circuit voltage are identical. For real solar cells $\mu \approx qV_{OC}$ only when there is no bending of the quasi-Fermi levels and each of them aligns with the respective electrode work function and when devices are operated at moderate light intensities.^[19,21]

In this work, we prepare efficient p–i–n perovskite solar cells incorporating Cs^+ , methyl-ammonium, and alpha-methylbenzyl ammonium iodide cations. This leads to a quasi-2D perovskite absorber with excellent photo-physical properties. Solar cells packaged between glass slides show excellent stability under white-light illumination. We study the optical properties of the synthesized absorber layer and characterize the solar cells in detail. We determine the ideality factor and build a simulation model that describes the basic device characteristics very well. Our findings show that the incorporated alpha-methylbenzyl ammonium iodide cation contributes to reduce the defect densities and improves the device V_{OC} and overall performance. Moreover, it suggests that the studied solar cell is

an excellent candidate for flexible applications or a subcell in a multijunction device.

2. Experimental Section

2.1. Materials

Chemicals and solvents were purchased from commercial suppliers and used as received, if not stated otherwise. Patterned indium tin oxide (ITO)-coated glass substrates ($15 \Omega \text{ cm}^{-2}$), glass slides, lead iodide (PbI_2 , Alfa Aesar, 99.9%), lead chloride (PbCl_2 , Sigma Aldrich, 99.9%),^[6,6]-phenyl-C61-butyric acid methyl ester (PCBM, nano-c), poly(3,4-ethylene dioxythiophene):polystyrene sulfonate (PEDOT:PSS, Clevis PH 1000), ZonylFS-300 fluorosurfactant (40% in H_2O , Fluka), methylammonium iodide ($\text{CH}_3\text{NH}_3\text{I}$), alpha-methylbenzylamine ($\text{C}_8\text{H}_9\text{NH}_2$, Sigma Aldrich), hydroiodic acid (HI, 57 wt%, Sigma Aldrich), aluminum, E131 encapsulation epoxy (Ossila), anhydrous N,N -dimethylformamide (DMF, Sigma Aldrich), dimethylsulfoxide (DMSO, Anal. R. VWR Chemicals, 99.5 %), chlorobenzene ($\text{C}_6\text{H}_5\text{Cl}$, 99.8 %, Sigma Aldrich), acetone (VWR Chemicals), ethanol (absolute for analysis, Merck), isopropanol (VWR Chemicals), Hellmanex III detergent (Hellma Analytics), and acetylacetone ($\text{CH}_3\text{COCH}_2\text{COCH}_3$, Sigma Aldrich, $\geq 99\%$) were used.

2.2. Synthesis of Alpha-Methylbenzyl Ammonium Iodide

Alpha-methylbenzyl ammonium iodide (MBAI) salts were synthesized by mixing an equimolar amount of alpha-methylbenzylamine and hydroiodic acid (HI), in which alpha-methylbenzylamine was first added into a round-bottom flask and cooled in an ice bath to keep the reaction temperature at 0°C , then HI was added drop-by-drop with continuous stirring. The reaction mixture was diluted with ethanol (using twice the volume of HI used) and left under stirring in the ice bath for 2 h. The solvent was then evaporated using a rotary evaporator (BUCHI Rotavapor R-114 coupled with a BUCHI water bath B-480). The resulting crystals were redissolved in a small amount of ethanol and recrystallized by adding diethyl ether and decanted. Washing with diethyl ether was repeated until clean white crystals were obtained. The crystals were then filtered with a Buchner funnel under vacuum and transferred to a round bottom flask followed by freeze-drying. Finally, the dried, white powder of MBAI (Figure 1a) was transferred into a vial and kept in a nitrogen glove box. The synthesized salt was characterized using Fourier transform infrared spectroscopy and proton nuclear magnetic resonance spectrometer (Figure S1 and S2, Supporting Information). Methylammonium iodide (MAI) was synthesized following an analogous procedure used for MBAI.

2.3. PEDOT:PSS Solution Preparation

PEDOT:PSS solution was prepared by mixing Clevis PH1000 stock solution with 7 vol% DMSO and 0.7 vol% Zonyl FS-300, stirring at room temperature for an hour, and keeping at 4°C overnight. The PEDOT:PSS solution was filtered through a Minisart RC25 syringe filter ($0.45 \mu\text{m}$, regenerated cellulose) right before use.

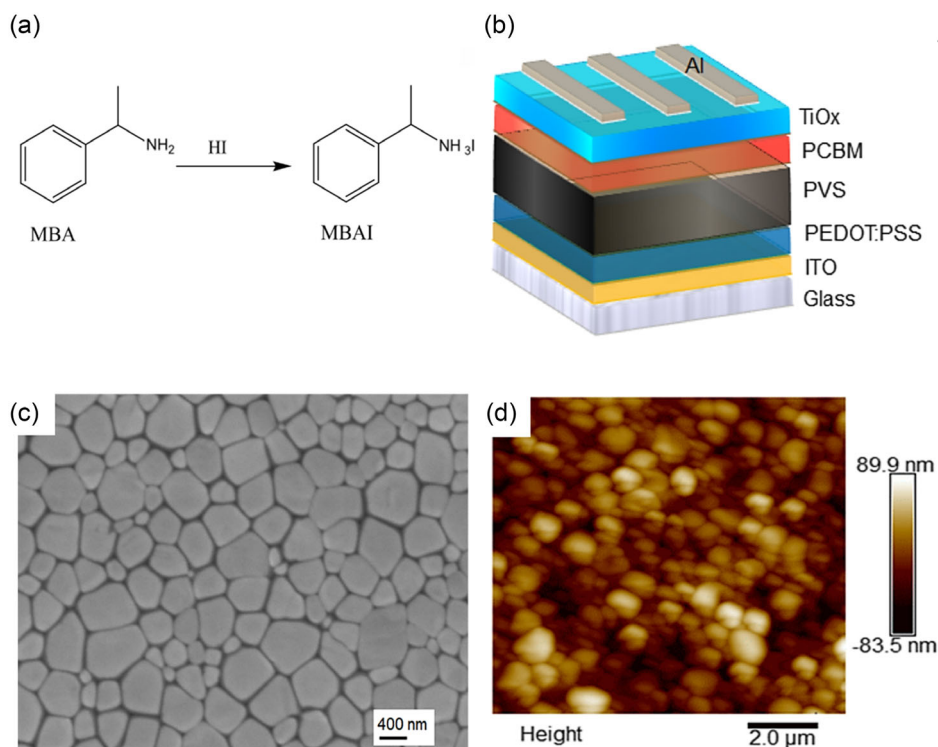


Figure 1. a) Chemical structure and synthesis route of alpha-methylbenzyl ammonium iodide (MBAI) from alpha-methylbenzylamine (MBA) and hydroiodic acid (HI). b) Schematics of the device structure. c) Topographic scanning electron microscope (SEM) image and d) atomic force microscope (AFM) image of quasi-2D perovskite film.

2.4. Perovskite Solution

Perovskite (PVS) solution ((MBA)₂(Cs_{0.12}MA_{0.88})₆Pb₇(I_xCl_{1-x})₂₂) was prepared by mixing PbI₂ (322.4 mg), PbCl₂ (83.5 mg), MBAI (74.7 mg), and MAI (187.8 mg) in 0.733 mL of DMF containing 10 vol% acetylacetone and stirred for 1 h at 55 °C. Afterward, CsI (≈0.12 mmol, from 1.5 M stock solution in DMSO) was added to the mixture and stirred for about 5 h. The solution was filtered using polytetrafluoroethylene (PTFE) syringe filters (0.45 μm; Whatman).

2.5. Device Fabrication

To fabricate the solar cells, prepatterned glass substrates coated with indium tin oxide (ITO) were sequentially sonicated in detergent, deionized water, acetone, and isopropanol (IPA). The hole transport layer PEDOT:PSS (Clevious PH1000) was spin-coated on cleaned glass/ITO substrates at 1500 rpm for 45 s and dried at 120 °C for 15 min which was followed by IPA washing via spin-coating at 4000 rpm for 15 s and heating at 120 °C for 15 min. Samples were transferred into a nitrogen glovebox for further processes. The perovskite solution was deposited on top of PEDOT:PSS films in two steps at: 1) 1000 rpm for 5 s with ramp: 200 rpm s⁻¹ and at; 2) 4000 rpm for 25 s with ramp: 2000 rpm s⁻¹, with in situ antisolvent quenching by dropping about 0.19 mL of chlorobenzene starting at the last 12th s. Then films were annealed at 100 °C for 1 h. After the samples

were cooled down to room temperature, 2 wt% PCBM dissolved in a mixture of chlorobenzene and chloroform (75:25 volume ratio, respectively) was spin-coated on top of the perovskite film. A TiO_x interlayer was spin-coated on top of PCBM at 5000 rpm for 30 s followed by annealing at 105 °C for about 7 min in ambient air. Devices were finalized by depositing aluminum through a shadow mask by thermal evaporation at a pressure of ≈10⁻⁶ mbar resulting in solar cells with active areas in the range of 0.15–0.2 cm².

For optical experiments, different layer stacks were deposited on glass substrates applying the same parameters used for device processing. Solar cells were encapsulated with a thin glass slide using UV-curable epoxy.

2.6. Solar Cell Characterization

Photovoltaic performance was evaluated using commercial solar simulators. The light intensity was matched to 1 sun (AM 1.5G or 100 mW cm⁻²) by calibration with a Si reference cell. The current–voltage (*j*–*V*) curves were collected by applying an external bias voltage while measuring the current response using a Keithley 2400 source meter unit. For maximum power point tracking a halogen lamp (Philips, GU5.3, 20 W, 3000 K) was used as an illumination source. Data were collected with a Keithley 2401 source meter unit and a homemade Python-based software tool. External quantum efficiencies (EQEs) were recorded using a lock-in amplifier (SR830, Stanford Research Systems) and a variable gain

preamplifier (Jaisle 1002 potentiostat or FEMTO DLPCA-200). Solar cells were illuminated by monochromatic light from a white light lamp passing through a monochromator with typical intensities in the range of 0.1–10 μW . A set of long-pass filters and a mechanical chopper were mounted between the lamp and the monochromator. Chopping frequencies in the range of 113–273 Hz were used. A calibrated silicon diode (Hamamatsu S2281) and a calibrated InGaAs diode (Hamamatsu G12180) were used as references. The electroluminescence quantum yield was determined using a calibrated EQE measurement system (Hamamatsu C9920-12). The system comprises an integrating sphere, a photonic multichannel analyzer (Hamamatsu PMA-12 C10027-02), and a Keithley 2400 source meter unit. For photoluminescence (PL) measurements, samples were excited with a diode laser (OBIS Coherent), and the sample's emission was collected with an optical lens and fed into a Shamrock monochromator (303-i) equipped with an Andor iDus420 CCD camera. For photoluminescence measurements, long-pass filters were used to block the high-energy photons from the excitation source. Fluorescence lifetimes were determined with a SPC-130 (Becker & Hickl) time-correlated single-photon counting set-up equipped with a monochromator (DeltaNu DNS-300, grating: 600 L mm^{-1} , 500 nm blaze). A supercontinuum white light laser equipped with a pulse picker (NKT Photonics SuperK extreme FIU-15) connected to the monochromator (Photonetc LLTF contrast) was used as an excitation source.

2.7. Solar Cell Modeling

Device simulations were performed using SCAPS 3.3.10. SCAPS is an open-source code and can be obtained from <https://user.s.elis.ugent.be/ELISgroups/solar/projects/scaps> upon the conditions requested by the developers Marc Burgelman et al. Simulation parameters and further details are discussed in the Supporting Information. Initial parameters were selected based on the model presented in previous studies.^[11,22,23]

3. Results and Discussion

The typical device architecture of the prepared perovskite solar cells is shown in Figure 1b. Typical layer thicknesses were found to be about 80 nm PEDOT:PSS, 400 nm of photoactive perovskite material, about 80 nm of PCBM, 10 nm of TiO_x , and about 100 nm of aluminum.

Figure 1c illustrates the typical surface morphology of the perovskite absorber material. Grains with a typical size of 100–1000 nm form a dense layer on a PEDOT:PSS layer, and AFM image (Figure 1d) shows the root-mean-square (RMS) roughness of the corresponding perovskite films is about 25 nm. Figure S3a, Supporting Information displays the optical transmission of different layer stacks utilized in the studied solar cells. The absorption of the photoactive perovskite layer ($\text{MBA}_2(\text{Cs}_{0.12}\text{MA}_{0.88})_6\text{Pb}_7\text{I}_{22}$) was measured using photothermal deflection spectroscopy to evaluate the optical bandgap. Figure S3b, Supporting Information presents the absorption spectrum and photoluminescence of the thin film. The bandgap estimated from the Tauc plot is ≈ 1.58 eV (Figure S3c, Supporting Information). In Figure 2a the current–voltage

(j – V) curves recorded at different light intensities are plotted. The white light intensity was adjusted such that the solar cell delivered a short circuit current equivalent to AM1.5G illumination. Optical density filters were mounted between the light source and the solar cell to change the white light intensity. The shown current–voltage curves were recorded by slowly scanning from negative to positive potentials with a scan rate of 30 mV s^{-1} . The studied solar cells show a weak dependence of the current–voltage curve on the scan direction (hysteresis) giving slightly higher power conversion efficiencies when the j – V -characteristic is recorded starting from positive potential. Figure 2b shows the EQE spectra recorded with and without dc-light bias. With a dc-bias-light inducing a photocurrent of $\approx 0.4 \text{ mA cm}^{-2}$ the EQE is slightly increasing suggesting that shallow traps are active in the device.

The presence of trap states is also supported by a weak absorption feature observed in the EQE spectrum at energies below the bandgap (Figure 2c). Such subgap defects have been found in different types of solar cells and are critical for the evaluation of open circuit voltage losses.^[24–26] Compared to typical n – i – p perovskite devices^[27,28] the EQE of the investigated devices is relatively low. This is also one of the main reasons for their moderate PCE. The transmission spectra shown in Figure S3, Supporting Information suggest that the relatively thick PEDOT:PSS layer is responsible for the reduced EQE in the near-infrared region as well as in the range of 400–500 nm.

The integral of the measured EQE spectrum multiplied by the AM1.5G spectrum gives a short circuit current of 17.9 mA cm^{-2} . With a fill factor of 74% and an open-circuit voltage of 1.13 V, the investigated solar cell has a PCE of $\approx 15\%$. Figure 2d shows the measured and simulated light intensity dependence of the open-circuit voltage and the fill factor. Even at low-light intensities, the devices show fill factors >0.7 leading to an extraordinary performance of the devices at low-light conditions. This suggests that such devices are highly promising for low-light and indoor light applications.

Figure 3a illustrates the excellent stability of the studied devices. Maximum power point tracking was performed under 1 sun white light equivalent illumination. The device maintains $>97\%$ of the initial performance after 500 h of operation. The tested solar cell was exposed to white light illumination for the entire time. Several devices based on the same layer stack have been tested under long-term illumination. Figure S4, Supporting Information shows the power output at the maximum power point of a similar solar cell recorded for 1000 h. Again excellent stability was observed for this device, maintaining above 97% of its initial output. In Figure 3b, the electroluminescence spectra recorded at different injection currents are shown. The electroluminescence quantum efficiency (ELQY) was typically in the range of 0.05% at injection currents comparable to photocurrents under AM1.5G illumination. In Figure 4a, the measured open circuit voltage plotted versus the short circuit current density (i_{sc}) is shown. In Figure 4b, the photoluminescence recorded at V_{OC} is shown. The solar cell was excited using monochromatic light (637 nm) from a diode laser. Plotting V_{OC} versus i_{sc} , the diode ideality factor $n = 1.46$ was found. Plotting the photoluminescence (PL) versus the V_{OC} a prefactor of 1.06 times $q/(k_{\text{B}}T)$ is obtained. This is consistent with the linear dependence of the

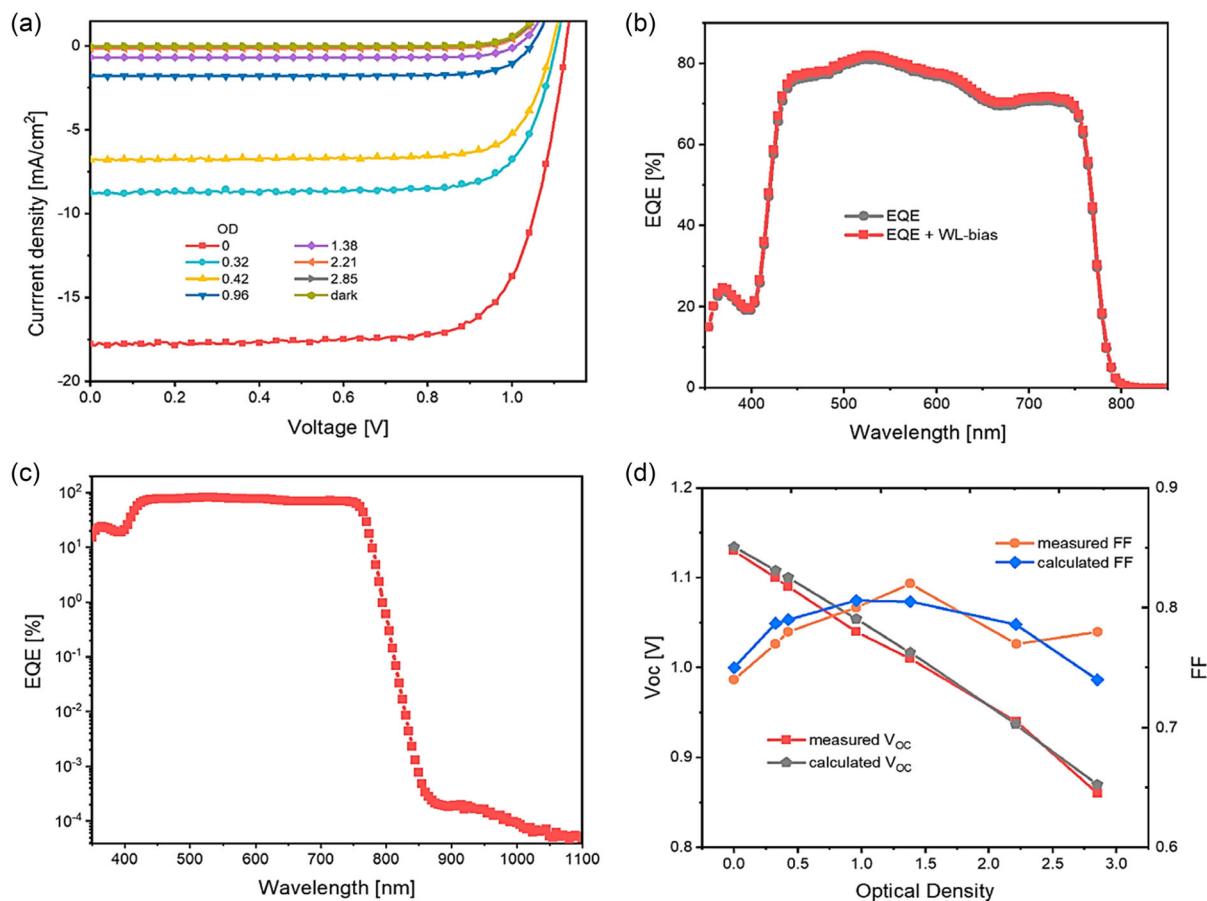


Figure 2. a) Current–voltage curves recorded at different illumination intensities. b) External quantum efficiency spectra recorded with and without back-light bias. c) High sensitivity EQE spectrum. d) Measured and calculated device parameters (open circuit voltage (V_{oc}) and fill factor (FF)) for different light intensities.

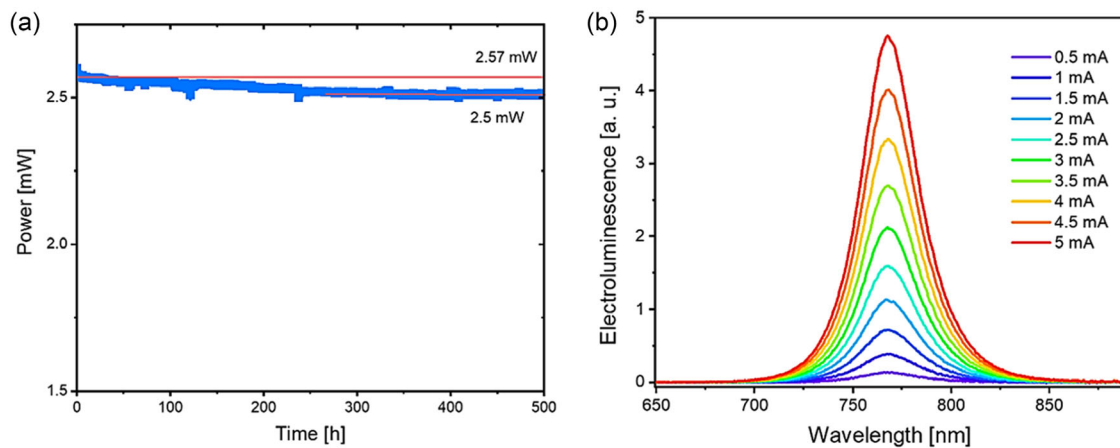


Figure 3. a) Maximum power point tracking under white light illumination. b) Electroluminescence spectra recorded at different injection currents.

short circuit current on the light intensity observed for the prepared devices. Figure 4c,d shows that the same data extracted from the performed SCAPS simulation. The compiled model predicts an ideality factor of around 1.48. The prefactor extracted

from PL versus V_{oc} is 0.99 times $q/(k_B T)$. In Figure S5, Supporting Information, the measured and simulated current–voltage curves recorded at different light intensities are compared, showing excellent matching.

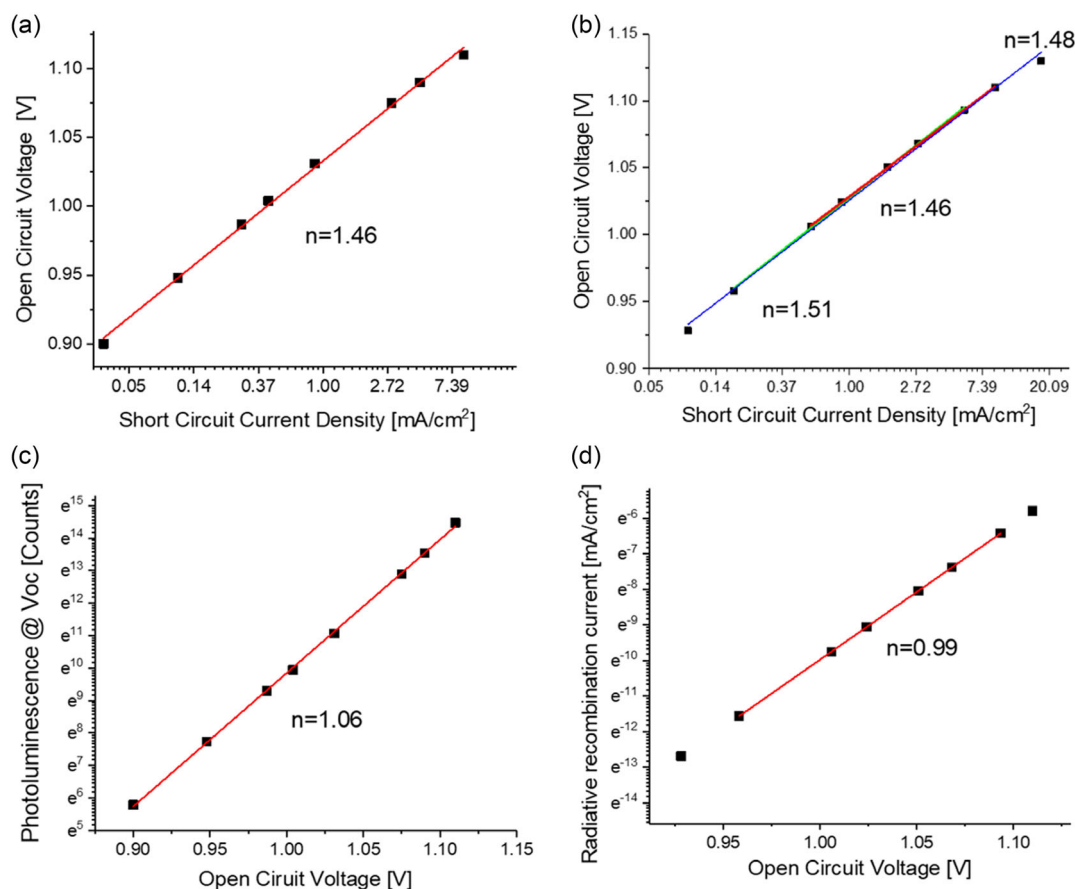


Figure 4. a) Measured open circuit voltage plotted versus the short circuit current density, b) measured photoluminescence plotted versus the open circuit voltage, c) calculated open circuit voltage plotted versus the short circuit current density, and d) calculated radiative recombination current plotted versus the open circuit voltage.

Overall, the SCAPS model does reproduce the device data well. However, to build the model, several material parameters and information about trap states and recombination processes are required, which are not available for the investigated perovskite material and device stack. Therefore, we applied material parameters available in the literature and modified trap densities, recombination parameters, energy levels, etc. to fit our experimental device data. To estimate the radiative recombination coefficient, the ELQY value of 0.05% was used to set the amplitude of the radiative recombination current. For the charge carrier lifetime in the perovskite absorber material, the long-lived component of the photoluminescence of a perovskite film deposited on a PEDOT:PSS was used (Figure S6a, Supporting Information). The defect properties in the perovskite are adjusted to obtain a charge carrier lifetime of ≈ 80 ns. In a device operated at V_{OC} or I_{SC} , the photoluminescence lifetime is found to be shorter (Figure S6b, Supporting Information). Additional surface recombination processes and the extraction of charge carriers lead to a faster decay of photo-induced charge carriers in the solar cell. As the photoluminescence measurements were performed at moderate excitation intensities ($\approx 1 \text{ mW cm}^{-2}$, 643 nm), the obtained decay times should reflect the decay dynamics at low charge carrier concentrations.

4. Summary

We have prepared and characterized quasi-2D *p-i-n* perovskite solar cells using MBAI as a large cation component and PEDOT:PSS as a hole transport layer. The incorporation of MBAI leads to films with excellent optical and electrical properties, leading to higher V_{OC} , FF, and stability of the device. A high open-circuit voltage and fill factor and corrected power conversion efficiencies in the range of 15% were obtained for the prepared devices. Encapsulated solar cells show excellent power output stability under white light illumination for >500 h. Due to the simple and robust preparation process, the investigated inverted perovskite solar cell can easily be combined with other solution-processed thin film solar cells to form multijunction devices and can easily be integrated into different lightweight and flexible products.

Supporting Information

Supporting Information is available from the Wiley Online Library or from the author.

Acknowledgements

B.H. acknowledges the financial support by the European Union's Horizon 2020 research and innovation program under grant agreement no. 101016411 "Soft Milli-robots-SOMIRO" and European Research Council (ERC) Starting Grant "GEL-SYS" under grant agreement no. 757931 to M.K. M.C.S. acknowledges financial support by the Austrian "Climate and Energy Fund" within the program Energy Emission Austria (Project: ALTAPOS, FFG No. 865072).

Conflict of Interest

The authors declare no conflict of interest.

Data Availability Statement

The data that support the findings of this study are available from the corresponding author upon reasonable request.

Keywords

solar cells, perovskites, device simulation, device stability

Received: April 28, 2023

Revised: June 4, 2023

Published online: August 30, 2023

- [1] A. Kojima, K. Teshima, Y. Shirai, T. Miyasaka, *J. Am. Chem. Soc.* **2009**, *131*, 6050.
- [2] National Renewable Energy Laboratory, <https://www.nrel.gov/pv/cell-efficiency.html> (accessed: February 2023).
- [3] M. A. Green, E. D. Dunlop, J. Hohl-Ebinger, M. Yoshita, N. Kopidakis, K. Bothe, D. Hinken, M. Rauer, X. Hao, *Prog. Photovoltaics Res. Appl.* **2022**, *30*, 687.
- [4] G. Adam, M. Kaltenbrunner, E. Daniel, D. Hazar, M. Schuette, H. Heilbrunner, S. Tombe, P. Stadler, B. Ernecker, C. Wolfgang, N. Serdar, M. C. Scharber, *Solar Energy Mater. Solar Cells* **2016**, *157*, 318.
- [5] S. S. Mali, Chang K. Hong, *Nanoscale* **2016**, *8*, 10528.
- [6] W. Han, G. Ren, J. Liu, Z. Li, H. Bao, C. Liu, W. Guo, *ACS Appl. Mater. Interfaces* **2020**, *12*, 49297.
- [7] Y. Xia, S. Dai, *J. Mater. Sci. Mater. Electron.* **2021**, *32*, 12746.
- [8] F. Wang, S. Bai, W. Tress, A. Hagfeldt, F. Gao, *npj Flex. Electron.* **2018**, *2*, 22.
- [9] Q. Cao, Y. Li, H. Zhang, Q. Cao, J. Yang, J. Han, T. Xu, S. Wang, Z. Wang, B. Gao, J. Zhao, X. Li, X. Ma, S. M. Zakeeruddin, W. E. I. Sha, X. Li, M. Grätzel, *Sci. Adv.* **2021**, *7*, eabg0633.
- [10] S. Xiong, Z. Hou, W. Dong, D. Li, J. Yang, R. Bai, Y. Wu, D. Li, H. Wu, Z. Ma, J. Xu, X. Liu, Q. Bao, *Adv. Energy Mater.* **2021**, *11*, 2101394.
- [11] M. Saliba, T. Matsui, J.-Y. Seo, K. Domanski, J.-P. Correa-Baena, M. K. Nazeeruddin, S. M. Zakeeruddin, W. Tress, A. Abate, A. Hagfeldt, M. Grätzel, *Energy Environ. Sci.* **2016**, *9*, 1989.
- [12] L. Zuo, H. Guo, D. W. DeQuilettes, S. Jariwala, N. De Marco, S. Dong, R. DeBlock, D. S. Ginger, B. Dunn, M. Wang, Y. Yang, *Sci. Adv.* **2017**, *3*, e1700106.
- [13] X. Wang, K. Rakstys, K. Jack, H. Jin, J. Lai, H. Li, C. S. K. Ranasinghe, J. Saghaei, G. R. Zhang, P. L. Burn, I. R. Gentle, P. E. Shaw, *Nat. Commun.* **2021**, *12*, 52.
- [14] X. Zheng, Y. Hou, C. Bao, J. Yin, F. Yuan, Z. Huang, K. Song, J. Liu, J. Troughton, N. Gasparini, *Nat. Energy* **2020**, *5*, 131.
- [15] G. Grancini, C. Roldán-Carmona, I. Zimmermann, E. Mosconi, X. Lee, D. Martineau, S. Narbey, F. Oswald, F. De Angelis, M. Graetzel, M. K. Nazeeruddin, *Nat. Commun.* **2017**, *8*, 15684.
- [16] D. Luo, W. Yang, Z. Wang, A. Sadhanala, Q. Hu, R. Su, R. Shivanna, G. F. Trindade, J. F. Watts, Z. Xu, T. Liu, K. Chen, F. Ye, P. Wu, L. Zhao, J. Wu, Y. Tu, Y. Zhang, X. Yang, W. Zhang, R. H. Friend, Q. Gong, H. J. Snaith, R. Zhu, *Science* **2018**, *360*, 1442.
- [17] W. Shockley, *Bell Syst. Tech. J.* **1949**, *28*, 435.
- [18] C. T. Sah, R. Noyce, W. Shockley, *Proc. IRE* **1957**, *45*, 1228.
- [19] P. Caprioglio, C. M. Wolff, O. J. Sandberg, A. Armin, B. Rech, S. Albrecht, D. Neher, M. Stolterfoht, *Adv. Energy Mater.* **2020**, *10*, 2000502.
- [20] G. O. Odunmbaku, S. Chen, B. Guo, Y. Zhou, N. A. N. Ouedraogo, Y. Zheng, J. Li, M. Li, K. Sun, *Adv. Mater. Interfaces* **2022**, *9*, 2102137.
- [21] P. Caprioglio, M. Stolterfoht, C. M. Wolff, T. Unold, B. Rech, S. Albrecht, D. Neher, *Adv. Energy Mater.* **2019**, *9*, 1901631.
- [22] J. Diekmann, P. Caprioglio, M. H. Futscher, V. M. Le Corre, S. Reichert, F. Jaiser, M. Arvind, L. P. Toro, E. Gutierrez-Partida, F. Peña-Camargo, C. Deibel, B. Ehrler, T. Unold, T. Kirchartz, D. Neher, M. Stolterfoht, *Sol. RRL* **2021**, *5*, 2100219.
- [23] Y. He, L. Xu, C. Yang, X. Guo, S. Li, *Nanomaterials* **2021**, *11*, 2321.
- [24] J. Warby, F. Zu, S. Zeiske, E. Gutierrez-Partida, L. Frohloff, S. Kahmann, K. Frohna, E. Mosconi, E. Radicchi, F. Lang, S. Shah, F. Peña-Camargo, H. Hempel, T. Unold, N. Koch, A. Armin, F. De Angelis, S. D. Stranks, D. Neher, M. Stolterfoht, *Adv. Energy Mater.* **2022**, *12*, 2103567.
- [25] T. Leijtens, G. E. Eperon, A. J. Barker, G. Grancini, W. Zhang, J. M. Ball, A. R. S. Kandada, H. J. Snaith, A. Petrozz, *Energy Environ. Sci.* **2016**, *9*, 3472.
- [26] B. T. van Gorkom, T. P. A. van der Pol, K. Datta, M. M. Wien, R. A. J. Janssen, *Nat. Commun.* **2022**, *13*, 349.
- [27] S.-H. Turren-Cruz, A. Hagfeldt, M. Saliba, *Science* **2018**, *362*, 449.
- [28] Q. Jiang, Y. Zhao, X. Zhang, X. Yang, Y. Chen, Z. Chu, Q. Ye, X. Li, Z. Yin, J. You, *Nat. Photonics* **2019**, *13*, 460.